EXPERIMENTAL STUDY ON THE DAMPING RATIO OF A FLAT-ELLIPTICAL PIPE GREENHOUSE FRAME STRUCTURE
/
平椭圆管大棚骨架阻尼比测定试验研究

Cunxing WEI[1)], Hengyan XIE[2,*)], Xin ZHENG[2)], Wenbao XU[2)]
[1)] College of Engineering, Heilongjiang Bayi Agricultural University, Daqing 163319, China
[2)] College of Civil Engineering and Water Conservancy, Heilongjiang Bayi Agricultural University, Daqing 163319, China
Tel: +86-459-13766785587; E-mail: xiehy555@byau.cn
Corresponding author: Hengyan Xie
DOI: https://doi.org/10.35633/inmateh-77-38

Keywords: *greenhouse structure; excitation test; structural vibration; dynamic behavior; damping ratio*

ABSTRACT
Plastic greenhouses, due to their lightweight structural characteristics, often exhibit limited resistance to strong winds. To improve their wind-resistant performance, this study applied a combined approach using finite element modeling and excitation testing. Dynamic response data of the greenhouse frame were collected through excitation experiments, and frequency-amplitude characteristics were obtained using fast Fourier transform (FFT). Modal analysis of the finite element model was then performed to verify the experimental results, and the structural damping ratio was subsequently calculated. The results show that the acceleration amplitudes at the excitation point in the x- and z-directions were 1.66 and 1.25 times higher than those measured at adjacent frame sections, respectively. The natural frequency of the greenhouse frame was determined to be 3.15 Hz, and the corresponding damping ratio was 0.018. These findings provide insight into the dynamic behavior of flat-elliptical pipe greenhouse structures and offer a methodological reference for future structural optimization and the development of relevant engineering design standards.

摘要
塑料大棚由于其轻量化设计，在面对强风时的抵抗能力有限。为了提高其抗风性能，本文采用有限元法（FEM）和激振试验相结合的研究方法。通过激振试验获取大棚骨架的动态响应数据，利用快速傅里叶变换（FFT）提取幅频特性曲线，通过对骨架有限元模型进行模态分析，验证试验结果，最终计算得到结构的阻尼比。研究结果表明：激振骨架 x，z 向加速度幅值波动范围分别为相邻骨架的 1.66 倍和 1.25 倍，此类大棚骨架的自振频率为 3.15Hz，阻尼比为 0.018。这些结果有助于更深入地了解大棚骨架的结构动力学，并为未来的结构优化和设计标准制定提供方法论见解。

INTRODUCTION
Plastic greenhouses have become an essential component of modern agriculture, serving as one of the most widely adopted facilities for crop production *(Cheng, 2023; Xie, 2025)*. A typical greenhouse structure consists of the frame, film and film-tensioning line, among which the frame plays a critical role in maintaining overall structural stability and resisting external loads. The primary advantages of plastic greenhouses lie in their lightweight design and low construction cost *(Xie, 2025; Ha, 2017)*. However, these features also render the structures particularly vulnerable to extreme weather conditions, such as strong winds and heavy rainfall, with the frame being the most susceptible component. In recent years, the increasing frequency of extreme climatic events has amplified the impact of wind loads on plastic greenhouses, leading to frequent structural failures and collapses *(Briassoulis, 2016; Uematsu, 2020; Wang, 2025, Ryu, 2019).* To ensure structural safety and enhance resilience under adverse weather conditions, it is therefore imperative to conduct in-depth investigations into the wind-resistant performance of greenhouse frames.

Cunxing Wei, Ph.D. Eng.; Hengyan Xie, Prof. Ph.D. Eng.; Xin Zheng, Prof. Ph.D. Eng.; Wenbao Xu, Ph.D. Eng.

At present, the finite element method (FEM) is one of the most commonly used numerical approaches for investigating the wind-resistant performance of greenhouse frames. By constructing finite element models of the frame, researchers can conduct precise numerical simulations of both the global structural behavior and local details. Wind loads are typically represented as concentrated or distributed forces applied to the frame, enabling the evaluation of its deformation and stress distribution under different loading conditions *(Ren, 2019, Dougka, 2020)*. This method not only helps to identify potential weak points in the frame but also provides a scientific basis for structural optimization *(Liu, 2021; Wang, 2022; Wang, 2023)*. However, conventional FEM analyses often assume wind loads to be uniform or constant, without fully accounting for the fluctuating characteristics of wind speed *(Reichrath, 2002; Kwon, 2016)*. To better approximate realistic wind conditions, some studies have adopted the harmonic superposition method to simulate fluctuating wind loads. By decomposing the frequency components of wind forces and superimposing them, this approach can more accurately reproduce the dynamic effects of natural wind on the frame, thereby significantly improving the fidelity of wind load simulations *(Wang, 2021; Li, 2022; Jiang, 2021)*.

In addition, research integrating random vibration theory has gradually been applied, further enhancing the ability to predict the effects of randomness and uncertainty in wind loads on structural responses. Nevertheless, despite the significant advantages of FEM in numerical simulations, it still faces certain limitations. In particular, challenges arise when accounting for complex factors such as realistic wind load characteristics, material nonlinearity, and contact behavior of connections, which may introduce errors. As a result, discrepancies can occur between simulation results and actual engineering performance. To more accurately evaluate the wind-resistant performance of greenhouse frames under real wind conditions, excitation testing has emerged as a valuable experimental approach. By directly capturing the dynamic responses of structures, it provides an effective complement to the limitations of FEM.

This study aims to gain deeper insight into the dynamic response of greenhouse frames under wind loading by integrating excitation testing with the finite element method (FEM). While FEM-based studies have been extensively used in the past, they often rely solely on numerical simulations that do not fully replicate the actual wind load effects on the structure. By incorporating experimental validation using excitation testing with flat-elliptical pipes, this study offers a novel approach to better match experimental results with simulation data. The combined use of FEM and excitation testing enables more accurate validation of the numerical models and enhances the reliability of the predictions for greenhouse frame performance under real-world wind conditions.

MATERIALS AND METHODS

Vibration theory applied to frames excitation tests

To investigate the dynamic response of the greenhouse frame under external excitation, the structural vibration process is modeled as a linear single-degree-of-freedom (SDOF) system. The system is represented by a mass-spring-damper model, according to Newton's second law, the governing equation of motion can be expressed as:

$$M\ddot{x}(t) + C\dot{x}(t) + Kx(t) = F(t) \tag{1}$$

where, M is the equivalent mass of the greenhouse frames at the test point; C is linear viscous damping coefficient; K is equivalent stiffness of the structural system; $\ddot{x}(t)$ is the acceleration; $\dot{x}(t)$ is the velocity and $x(t)$ is the displacement response; $F(t)$ is external excitation force acting on the system.

In practical applications, energy dissipation in greenhouse frame arises not only from the inherent material damping but also from factors such as joint friction, air resistance, and internal friction due to material deformation. Thus, the free vibration process of a specific point on the frame can be approximated as damped vibration. The characteristic equation of the damped system determines whether the structure is in an overdamped, critically damped, or underdamped state. The critical damping coefficient is defined as:

$$C_{cr} = 2\sqrt{mk} \tag{2}$$

The damping ratio is defined as:

$$\zeta = \frac{c}{c_{cr}} \tag{3}$$

For structural vibration analysis, the underdamped case ($\zeta < 1$) is typically considered, as it exhibits oscillatory behavior. In this case, the damped natural frequency is given by:

$$\omega_d = \omega_n \sqrt{1-\zeta^2} \tag{4}$$

$$\omega_n = \sqrt{\frac{k}{m}} \tag{5}$$

where, ω_n is the undamped natural frequency. The displacement response can be expressed as:

$$x(t) = X_0 e^{-\zeta\omega_n t} \sin(\omega_d t + \phi) \tag{6}$$

where, X_0 is the initial amplitude and X_0 is the initial phase angle. This equation shows that the structure oscillates at the damped frequency ω_d, and the amplitude decays exponentially within the envelope function.

In the experiment, the logarithmic decrement method is used to identify the natural frequency and damping ratio of the greenhouse frame. The logarithmic decrement δ is defined as:

$$\delta = \frac{1}{n} \ln\left(\frac{x(t)}{x(t+nT_d)}\right) \tag{7}$$

where, n is the number of oscillation cycles considered, $x(t)$ is the amplitude at the reference time, $x(t+nT_d)$ is the amplitude after n cycles, and $T_d = \frac{2\pi}{\omega_d}$ is the damped vibration period. The damping ratio ζ can then be calculated from δ.

When an impulsive load is applied to the frame, it imparts an initial velocity to the system. The subsequent response is primarily governed by the sinusoidal term in the displacement solution, reflecting the damped oscillatory behavior of the frame.

Greenhouse structure and material selection

The greenhouse investigated in this study is located at the vegetable greenhouse experimental base of Heilongjiang Bayi Agricultural University and adopts a plastic-covered structure with a flat-elliptical pipe frame. The greenhouse has an overall length of 50 m, a height of 3.6 m, and a span of 10 m. Its primary components consist of film-tensioning line, film, and the frame.

The frame steel pipes used for excitation in this study are galvanized Q235B flat-elliptical pipe, with a cross-sectional size of 30 mm × 60 mm and a wall thickness of 2 mm. The flat-elliptical pipe design is achieved by rounding the sharp corners of rectangular steel pipes. Compared with conventional rectangular pipes, this design not only reduces wear and abrasion on the greenhouse film, thereby lowering the risk of film damage, but also increases the outer contour area and the moment of inertia in the load-bearing direction. As a result, the stiffness and stability of the greenhouse frame are significantly enhanced.

In addition, the surface of the flat-elliptical pipe is galvanized to enhance corrosion resistance and improve the steel's durability against environmental degradation over long-term use. Compared with truss-type greenhouse structures of equivalent mass, frames constructed with flat-elliptical pipe exhibit significant advantages in terms of stiffness and load-bearing capacity *(Yan, 2022)*. This ensures that, during excitation testing, the frame can better withstand and transmit the applied forces, thereby guaranteeing the reliability and accuracy of the experimental data.

a) Panoramic view *b) Diagram of the frame cross-section*

Fig. 1 – Flat-elliptical pipe greenhouse

Material parameter

In this study, the frame is constructed from Q235B galvanized steel pipes, which offer superior strength, rigidity, and corrosion resistance, thereby ensuring adequate support for the film structure under wind loading conditions *(Shin, 2021)*. The material parameters of the flat-elliptical pipe frames are summarized in Table 1.

Table1

Material parameter of steel pipe

Material	*b*×*h or R* (mm)	*t* (mm)	ρ (kg/m^3)	f_y (MPa)	λ	E (MPa)
Rafter	30×60	2	7.85	235	0.28	2.1×10^5
Embedded steel pipe	30×80	2	7.85	235	0.28	2.1×10^5
Purlin	ϕ 20	2	7.85	235	0.28	2.1×10^5

where, b is the width of section; h is the depth of section; t is thickness of section; ρ is density; f_y is the yield strength of steel; λ is Poisson ratio of steel; E is elasticity modulus of steel.

Design and structure of the vibration excitation rig

To ensure that the exciter can continuously and stably deliver the required forces during testing, a dedicated excitation test rig was designed for this study. The test rig is structurally configured to effectively support and secure key components, including the excitation platform, support rods, and counterweights, thereby minimizing the influence of external disturbances and enabling precise transmission of the applied forces. The design also considers the mechanical properties of individual components, stiffness compatibility, and overall system stability, aiming to prevent any factors that could introduce experimental errors or compromise platform stability.

The specific structure of the vibration excitation platform is illustrated in Fig. 2, showing the arrangement of its components and key dimensions. This configuration ensures that the entire excitation system achieves optimal mechanical performance during the testing process.

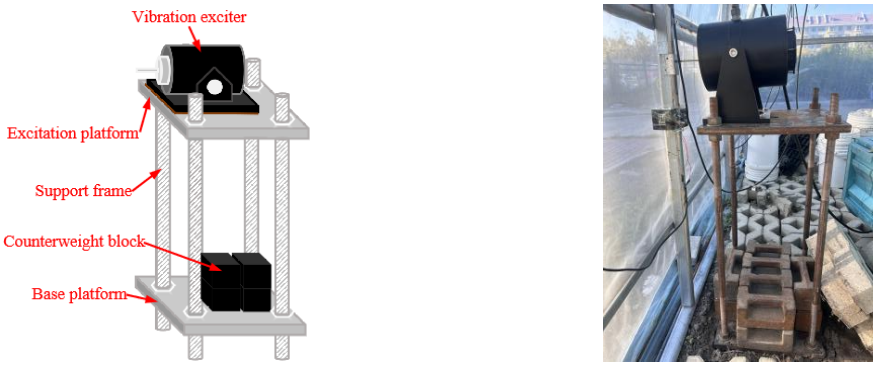

a) Schematic diagram *b) Physical picture*

Fig. 2 – Vibration excitation platform

Excitation platform: The excitation platform serves as the core component of the entire test rig, primarily responsible for transmitting the stiffness provided by the underlying support elements and for bearing and securing the exciter. In this study, the excitation platform was constructed from a 400 mm × 400 mm iron plate with a thickness of 20 mm. The thickness and mass of the plate were precisely calculated to meet the experimental requirements for stiffness and mass characteristics. The platform is connected to the underlying support rods via bolted joints, ensuring that no displacement or deformation occurs during testing, thereby enhancing the stability and accuracy of the experiment.

Support rods: The support rods play a critical role in the excitation test rig, primarily functioning to transmit the stiffness provided by the base platform and counterweights to the excitation platform, thereby ensuring the stability of the exciter during testing and preventing the generation of unintended vibrations. In this study, 4 threaded steel rods with a diameter of 20 mm were used as support rods. The threaded steel provides high strength and good bending resistance, effectively bearing the reaction forces generated during excitation. Moreover, the uniformity and strength of the material help prevent structural instability or vibrational resonance caused by stress concentrations.

Counterweights block: The counterweight is primarily used to adjust the system's center of gravity and mass distribution, thereby ensuring the stability of the excitation platform. In this study, 12 counterweights blocks, each weighing 5 kg, were evenly distributed on the base platform. This configuration optimizes the mass distribution of the test rig, ensuring platform balance during vibration and preventing instability due to uneven mass distribution.

Base platform: The base platform serves as the foundational component of the excitation test rig, primarily supporting the excitation platform, support rods, and counterweight blocks, while providing stable support for the entire excitation system. In this study, a steel plate of the same material as the excitation platform was selected as the base platform. This design ensures that the base platform's stiffness and mass distribution are consistent with those of the excitation platform, leading to a more uniform dynamic response of the entire system and effectively avoiding instability caused by material differences or mismatched stiffness.

Experimental Equipment and Testing Procedure

As shown in Fig. 3, the excitation system was provided by Yangzhou Jingming Technology Co., Ltd. and primarily consists of a JM1230 programmable digital signal generator, a JM5808 power amplifier, and a JMJ-50 vibration exciter. This system enables precise signal control to apply vibrational excitation to the greenhouse frame under study. The frame's acceleration was measured using a data acquisition system supplied by Jiangsu Donghua Testing Technology Co., Ltd., which includes DH2D001 accelerometers and a DH5922D dynamic signal acquisition analyzer.

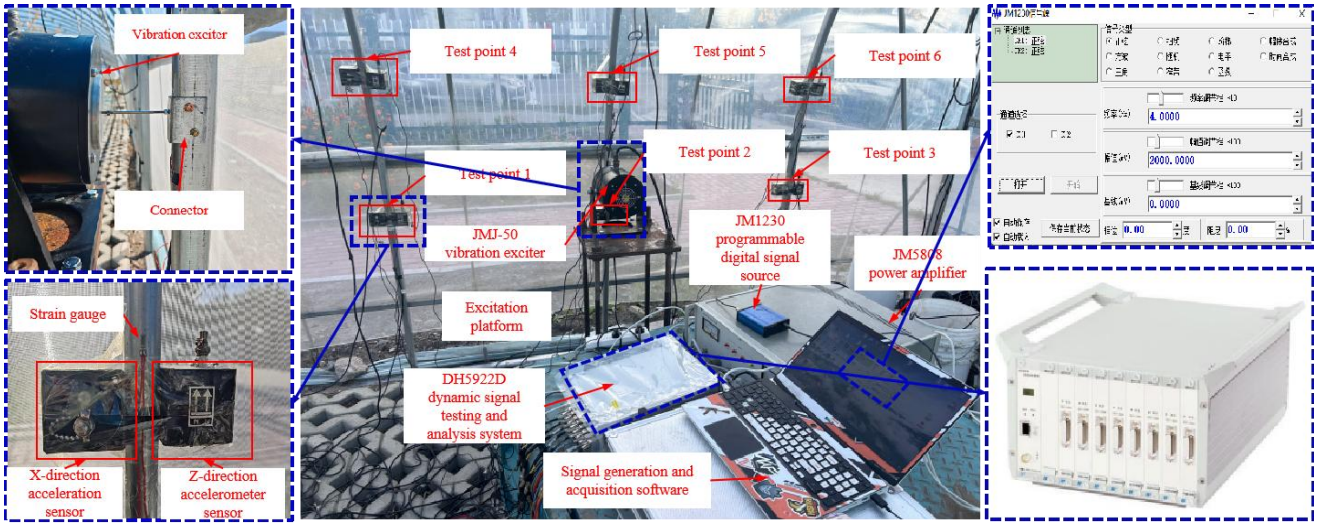

Fig. 3 – Experimental equipment

The experimental procedure was divided into a preparation stage and a testing stage. During the preparation stage, test points were first determined, and accelerometers were installed at the corresponding locations. Accelerometers were connected to the DH5922D data acquisition system via dedicated cables to enable real-time recording of the frame's acceleration response under excitation. Specifically, accelerometers were installed along the x-axis and z-axis, with the x-direction aligned with the main excitation direction of the exciter and the z-direction perpendicular to it. Once all sensors were installed, the excitation test rig was positioned at the designated location. To ensure that the exciter remained perpendicular to the frame throughout the excitation process, sleeves were mounted on the frame to fix the contact points of the exciter on the frame, thereby guaranteeing the accuracy of the excitation direction. At this point, the preparation stage was complete, and the system was ready to proceed to the testing stage.

During the testing stage, the JM1230 signal generator, operated via a PC, was first activated. The signal generator produced the desired excitation signal, which was transmitted to the JM5808 power amplifier. After amplification, the signal was delivered to the JMJ-50 vibration exciter, which ultimately output a sinusoidal excitation signal with a frequency of 4 Hz and an amplitude of 83.5 N, as shown in Fig. 4 This sinusoidal excitation was applied within a frequency range close to the natural frequency of the test object in order to investigate its natural frequency and damping characteristics.

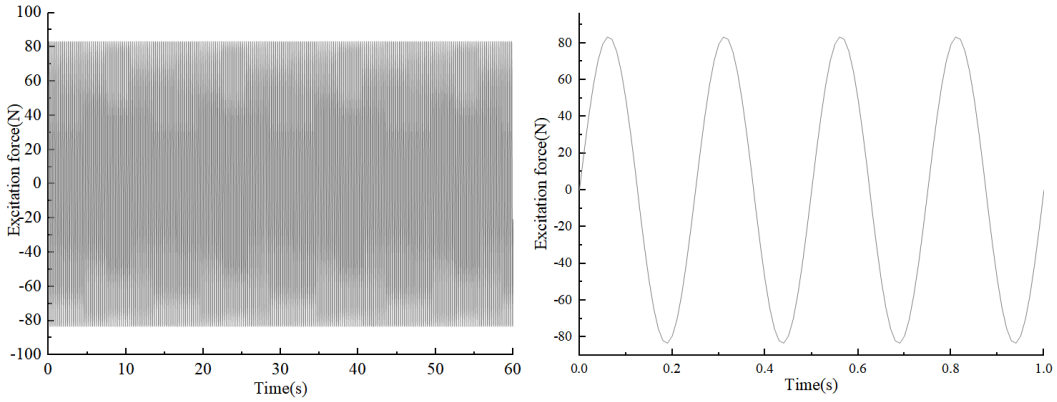

Fig. 4 – Excitation force time history curve

During this process, the DHDAS dynamic signal acquisition and analysis system was activated synchronously with the experimental equipment. Accelerometers mounted on the frame continuously monitored and recorded the acceleration responses at multiple points, and these data were transmitted in real time to the DHDAS system for storage and analysis, thereby completing the data acquisition process.

Measurement Uncertainty and Calibration Procedures

Before the excitation testing, all accelerometers were calibrated using a standard reference vibration calibrator with a known amplitude and frequency. The calibration ensured that the sensitivity deviation of each accelerometer was within ±2%. The data acquisition system was also verified by applying a reference sinusoidal signal to confirm linear response behavior and eliminate potential phase delays. During testing, repeated measurements were conducted under identical conditions to assess measurement repeatability. The overall uncertainty of acceleration measurement was estimated to be less than 3%, ensuring the reliability and accuracy of the recorded dynamic response data.

Data processing

During the experiment, acceleration signals from the system were continuously acquired in real time using the DHDAS dynamic signal acquisition system, with a sampling frequency set at 100 Hz to ensure high-precision recording. This data acquisition setup allows the capture of subtle dynamic variations during excitation, providing a reliable basis for subsequent frequency-domain analysis.

For data processing, the acquired time-domain signals were transformed into the frequency domain using the fast Fourier transform (FFT) to identify the system's natural frequencies and damping characteristics.

FFT parameters were chosen with a Hanning window and 50% overlap to minimize spectral leakage and improve frequency resolution. By analyzing the amplitude decay under different excitation modes, the damping ratio was further calculated using the logarithmic decrement method. Specifically, the amplitude decay over time during excitation was monitored, and an exponential decay model was fitted to the observed attenuation to determine the system's damping ratio. The diagram of data processing steps is shown in Fig. 5. This approach provides an accurate representation of the dynamic response of the greenhouse frame under excitation, thereby offering reliable data to support subsequent structural optimization and dynamic performance improvements.

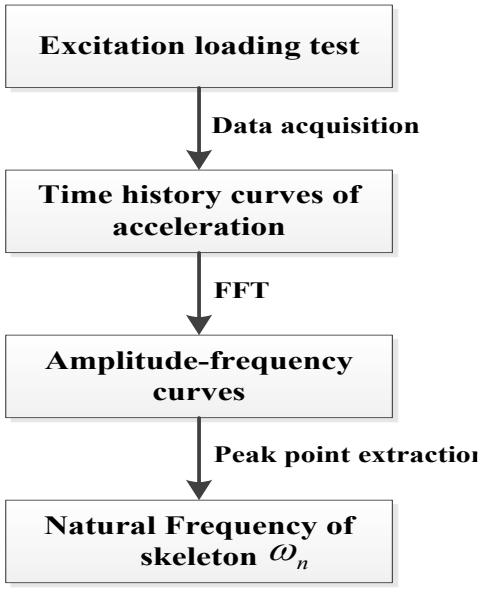

Fig. 5 – Diagram of data processing steps

RESULTS AND DISCUSSION

Time history analysis of acceleration

The acceleration time-history curves in the x- and z-directions at various test points of the frame, obtained using the DHDAS dynamic signal acquisition and analysis system, are shown in Fig. 6.

As shown in Fig. 6(a), the plots illustrate the acceleration responses in the x-direction and z-direction at different test points of the frame throughout the excitation process. In the Fig. 6, the blue curves represent the x-direction acceleration, while the red curves correspond to the z-direction acceleration. The left panels display the full acceleration time histories within 60 s, whereas the right panels provide detailed views of the interval from 30 s to 31 s. From the left panels, it is evident that the x-direction acceleration exhibits larger amplitude fluctuations throughout the test, whereas the z-direction acceleration shows comparatively smaller variations. This observation indicates a significant difference in the acceleration response of the flat-elliptical pipe greenhouse frame under sinusoidal excitation between the x-direction and z-direction, with a stronger response in the x-direction. Such differences are likely related to the geometry of the frame and its directional stiffness characteristics.

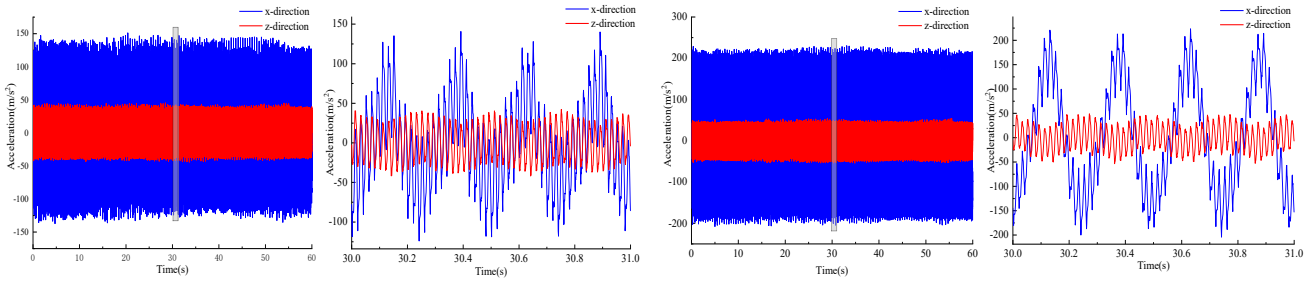

a) Test point 1 *b) Test point 2*

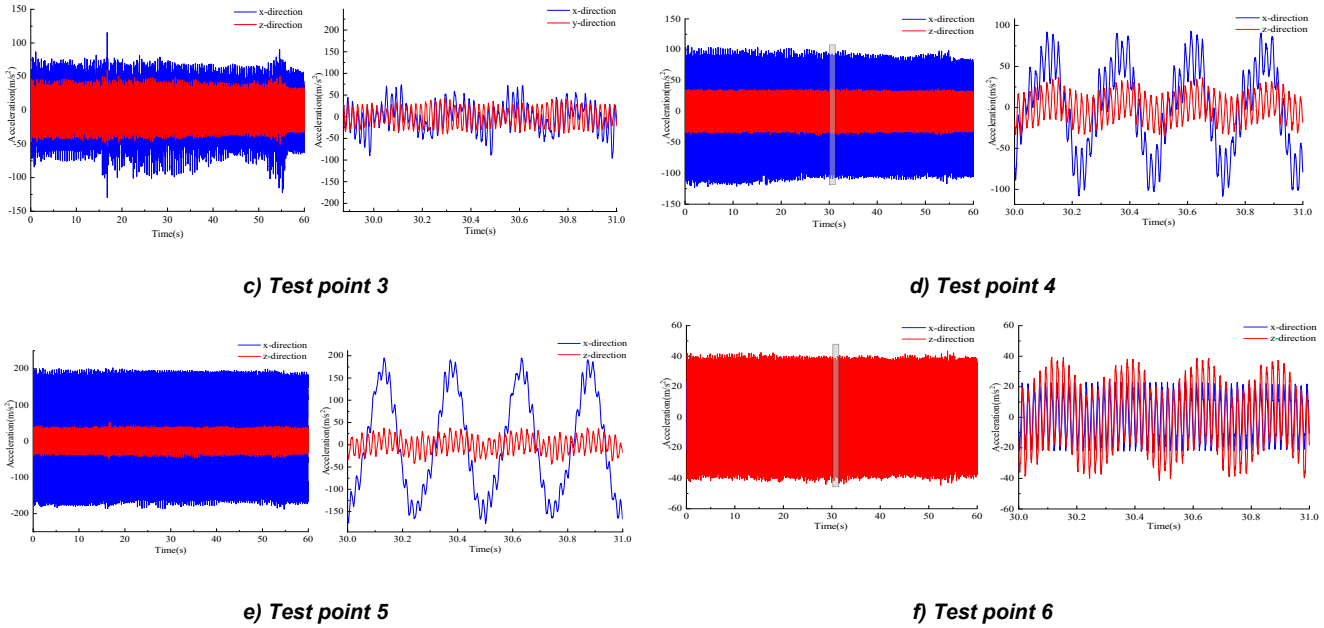

c) Test point 3 *d) Test point 4*

e) Test point 5 *f) Test point 6*

Fig. 6 – Acceleration time history curves of each test point

The discrepancies observed in the acceleration responses between the excited frame and adjacent frames could be attributed to several physical factors. Joint friction, for instance, may cause local damping effects, influencing the overall dynamic response. Additionally, boundary conditions such as fixed supports and material nonlinearity (e.g., yielding or buckling of the frame under certain load conditions) could result in deviations from the idealized behavior assumed in the finite element model. These factors may explain the variations observed in the amplitude of acceleration, particularly in the z-direction, where smaller fluctuations were noted compared to the x-direction.

By comparing the magnified x-direction and z-direction acceleration curves, a high degree of synchronization and periodicity is observed. Given that a 4 Hz sinusoidal excitation with an amplitude of 83.5 N was applied in this study, the x-direction and z-direction acceleration time histories clearly reflect the excitation frequency and waveform. Specifically, within a 1 s interval, 4 peaks corresponding to 4 complete sinusoidal cycles appear, reflecting the system's dynamic response characteristics and suggesting the presence of stable vibration modes or resonance phenomena. The observed synchronization of these periodic fluctuations further supports the notion of coordinated internal responses within the system during excitation.

Similarly, in Fig. 6(b), the x-direction and z-direction acceleration curves exhibit characteristics consistent with those observed in Fig. 6(a), displaying clear periodic fluctuations. Notably, the x-direction acceleration in Fig. 6(b) fluctuates between ±250 m/s², which is significantly larger than the ±150 m/s² range observed in Fig. 6(a), approximately 1.66 times greater. The z-direction acceleration in Fig. 6(b) primarily falls within ±50 m/s², slightly higher than the ±40 m/s² range in Fig. 6(a), about 1.25 times greater. These observations indicate that the acceleration time histories vary across different frames during the excitation test, with the frame subjected to direct excitation exhibiting significantly larger acceleration amplitudes than adjacent frames.

In summary, the system's dynamic response exhibited regular periodic variations, reflecting potential stability and synchronized behavior during the excitation process. These observations provide important reference data for subsequent dynamic modeling and system optimization. The present experiment thus offers critical experimental support for future structural improvements and dynamic response analyses.

Frequency domain analysis

The acceleration time-history curves at each test point were transformed into the frequency domain using the fast Fourier transform (FFT), and the resulting amplitude–frequency spectra for all test points are presented in Fig. 7.

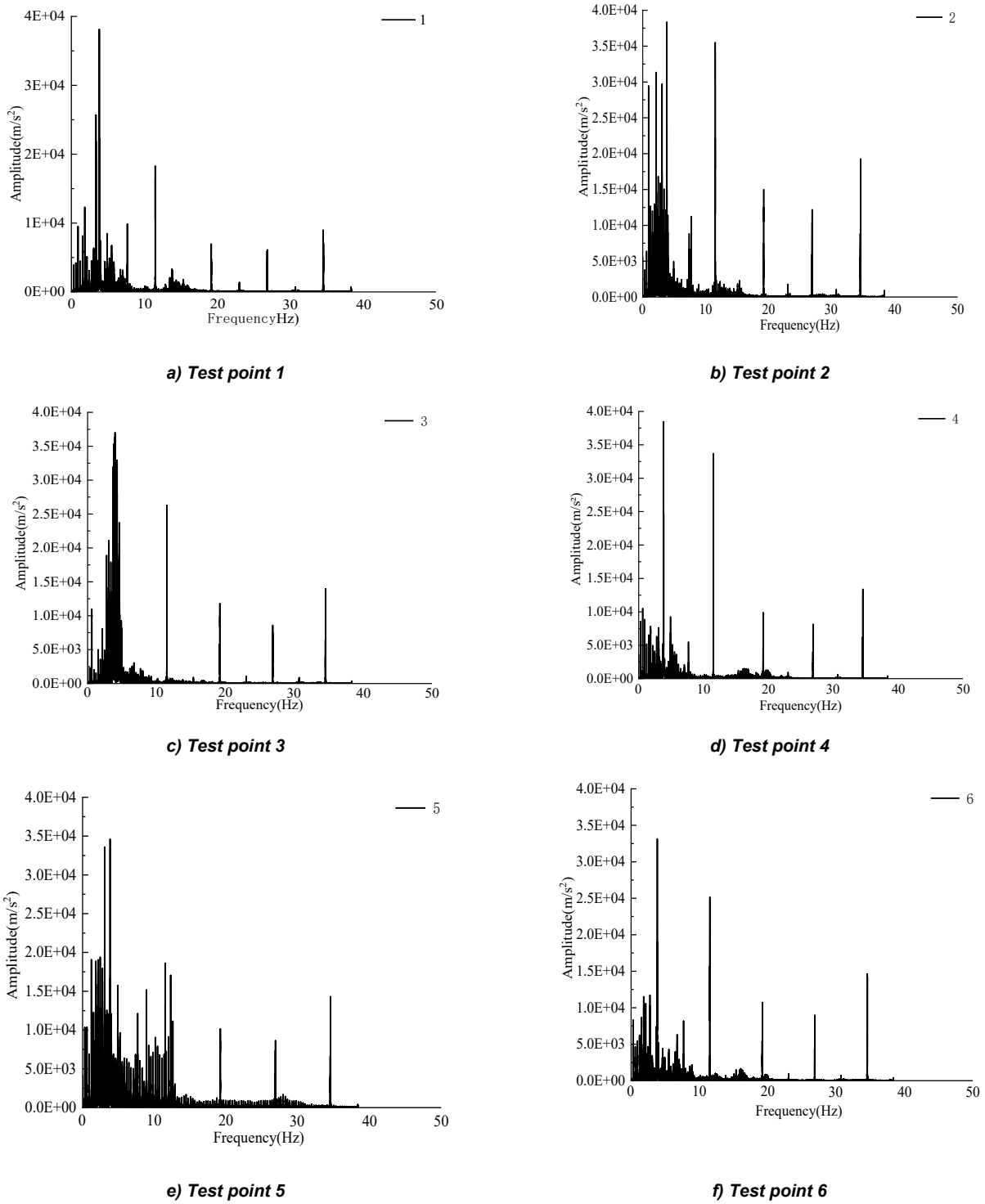

a) Test point 1 *b) Test point 2*

c) Test point 3 *d) Test point 4*

e) Test point 5 *f) Test point 6*

Fig. 7 – Amplitude-frequency curves of each test point

As shown in Fig. 7, the dominant frequencies at all test points fall within the 3–5 Hz range, with the peak frequency concentrated around 3.15 Hz. This indicates that the natural frequency of the structure is approximately 3.15 Hz. To validate the natural frequency obtained from the excitation test, a 3D model of the flat-elliptical pipe greenhouse frame was developed using ABAQUS finite element software. Modal analysis was then performed to determine the first 5 mode shapes and corresponding natural frequencies of the greenhouse frame, as presented in Fig. 8 and Table 2.

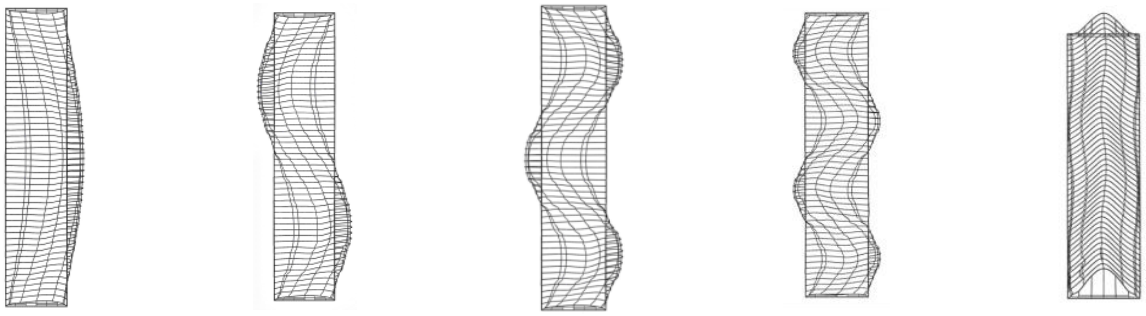

a) 1st vibration mode *b) 2nd vibration mode* *c) 3rd vibration mode* *d) 4th vibration mode* *e) 5th vibration mode*

Fig. 8 – The first 5 vibration modes of the structure

Table 2

First 5 natural frequencies of the structure

Mode order	1	2	3	4	5
Frequency/Hz	3.179	3.595	4.157	4.775	5.434

As shown in Table 2, the first-order natural frequency of the greenhouse frame obtained from the finite element model was 3.179 Hz, while the corresponding value determined from the excitation test was 3.15 Hz. The relative difference of 0.92% errors within the allowable range specified by the design code, indicating that the results of the excitation test are reliable.

Calculation of damping ratio

The damping ratio of the greenhouse frame was calculated using two methods: the logarithmic decrement method in the time domain and the half-power bandwidth method in the frequency domain. Based on the continuous excitation signals applied to the frame by the exciter during the experiment, and considering that the test did not involve a complete free decay process, the damping ratio was calculated using the frequency-domain half-power bandwidth method. The damping ratio of the greenhouse frame was determined to be 0.018.

$$\xi = \frac{\Delta f}{2 f_0} = \frac{3.2034 - 3.09}{2 \times 3.15} = 0.018 \tag{8}$$

where, ξ is damping ratio; Δf is the half-power bandwidth. On the frequency–amplitude curve, it is represented by the difference between the frequencies on either side of the resonance peak where the vibration amplitude reaches half of its maximum; f_0 is the natural frequency of the structure, corresponds to the frequency at which the maximum peak occurs on the frequency–amplitude curve.

CONCLUSIONS

This study focused on the dynamic response of a novel flat-elliptical pipe greenhouse subjected to excitation, combining experimental vibration testing with finite element analysis. Time-history analyses of acceleration at various test points were conducted, and the results were transformed into frequency–amplitude curves via FFT for frequency-domain analysis. The main conclusions are as follows:

(1) The excitation tests revealed significant differences in acceleration responses along the x-direction and z-direction of the greenhouse frame. At the test points located on the excited frame, the amplitude ranges of the x-direction and z-direction accelerations were 1.66 and 1.25 times greater than those at adjacent frames, respectively.

(2) The main frequency range observed in the frequency–amplitude curves was 3–5 Hz, with the peak frequency concentrated at 3.15 Hz. Modal analysis of the finite element model showed good agreement between the calculated natural frequencies and the experimental results.

(3) The damping ratio of this type of greenhouse frame, calculated using the structural damping formula, was determined to be 0.018.

This study provides a scientific basis for assessing the disaster resistance of such greenhouses under extreme weather conditions and offers data support for the development of mitigation measures and design standards. Notable variations were observed in the acceleration time-history curves, which may be linked to specific excitation events or external disturbances. Further investigation is needed to address potential noise effects or nonlinear responses.

Future work should focus on dynamic load testing under real wind or snow conditions to better understand greenhouse performance in realistic environments. Structural modifications to optimize damping could also enhance resilience. The findings provide valuable insights for improving greenhouse design, particularly in terms of wind resistance and structural stability, and offer a foundation for future design standards and mitigation strategies.

ACKNOWLEDGEMENTS

This study is supported by Natural Science Foundation of Heilongjiang Province of China (LH2019E072). All authors are grateful for this support.

REFERENCES

[1] Briassoulis. D., Dougka, G., Dimakogianni, D., & Vayas, I., (2016). Analysis of the collapse of a greenhouse with vaulted roof. *Biosystems Engineering*, Vol.151, pp. 495-509, England. DOI: https://doi.org/10.1016/j.biosystemseng.2016.10.018

[2] Cheng W., Wang Y., Wang C., Wang T., He J., Liu Z., Xu Y., (2023). Study on the variation of thermal environment and photosynthesis characteristics of strawberry in a solar greenhouse, *INMATEH - Agricultural Engineering*, Vol. 70, pp. 211-220, Bucharest/Romania. DOI: https://doi.org/10.35633/inmateh-70-21

[3] Dougka, G, Briassoulis. D., (2020). Load carrying capacity of greenhouse covering films under wind action: Optimising the supporting systems of greenhouse films. *Biosystems Engineering,* Vol. 192, pp, 199 -214, England. DOI: https://doi.org/10.1016/j.biosystemseng.2020.01.020

[4] Jiang Y., Bai Y., Wang C., Wang Y., Pang X., (2021). Dynamic response analyses of plastic greenhouse structure considering fluctuating wind Load. *Advances in Civil Engineering*. Vol. 2021, pp. 1-13, Egypt. DOI: https://doi.org/10.1155/2021/8886557

[5] Ha, T., Kim, J., Cho, B-H., Kim, D-J. (2017). Finite element model updating of multi-span greenhouses based on ambient vibration measurements. *Biosystems Engineering*, Vol. 161, pp. 145-156, England. DOI: https://doi.org/10.1016/j.biosystemseng.2017.06.019

[6] Kwon, K.-S., (2016). Evaluation of wind pressure coefficients of single-span greenhouses built on reclaimed coastal land using a large-sized wind tunnel. *Journal of Wind Engineering & Industrial Aerodynamics.* Vol. 141 pp. 58-81, England. DOI: https://doi.org/10.1016/j.biosystemseng.2015.11.007

[7] Li, X., Wang C., Jiang Y., Bai, Y., (2022). Dynamic response analysis of a whole steel frame solar greenhouse under wind loads. *Scientific reports*. Vol. 12, pp. 1-12, England. DOI: https://doi.org/10.1038/s41598-022-09248-z

[8] Liu X., Li Z., Liu Y., Li Y., Li T., (2021). Effect of single tube sections on the structural safety of Chinese solar greenhouse skeletons. *Scientific reports*. Vol. 11, No.119307. England. DOI: https://doi.org/10.1038/s41598-021-98779-y

[9] Ren, J., Wang, J., Guo, S., Li, X., Zheng, K., & Zhao, Z., (2019). Finite element analysis of the static properties and stability of a large-span plastic greenhouse. *Computers and Electronics in Agriculture.* Vol. 165, pp. 1-9, England. DOI: https://doi.org/10.1016/j.compag.2019.104957

[10] Reichrath, S., Davies, T., (2002). Computational fluid dynamics simulations and validation of the pressure distribution on the roof of a commercial multi-span Venlo-type glasshouse. *Journal of Wind Engineering and Industrial Aerodynamics*, Vol. 90, No. 3, pp. 139–149. England. https://doi.org/10.1016/s0167-6105(01)00184-2

[11] Ryu, H R., Choi, M K., Cho, M W. (2019). Damage index estimation by analysis of meteorological disasters on film plastic greenhouses. *International Journal of Agricultural and Biological Engineering*, Vol. 12, pp. 58-63. China. DOI: https://doi.org/10.25165/j.ijabe.20191205.4493

[12] Shin, H. H., Ryu, H. R., Yu, I. H., Cho, M. W., Seo, T. C., Kim, S. Y., & Choi, M. K., (2021). Effect of the Pipe Joint on Structural Performance of a Single-span Greenhouse: A Full-scale Experimental and Numerical Study. *Journal of Bio-Environment Control*, Vol. 30, No. 4, pp. 410–418. Korea. DOI: https://doi.org/10.12791/ksbec.2021.30.4.410

[13] Uematsu, Y., & Takahashi, K., (2020). Collapse and reinforcement of pipe-framed greenhouse under static wind loading. *Journal of Civil Engineering and Architecture*, Vol. 14, pp. 583-594, United States. DOI: https://doi.org/10.17265/1934-7359/2020.11.001

[14] Wang, C., Jiang, Y., Li, X., Bai, Y., Wang, T., (2021). Wind-induced vibration response analysis of Chinese solar greenhouses. *Computers and Electronics in Agriculture*, Vol. 181, pp. 1-15. England. DOI: https://doi.org/10.1016/j.compag.2020.105954

[15] Wang, C., Jiang, Y., Wang, T., Xu Z., Bai, Y., (2022). Analysis of wind-induced responses of landing assembled Chinese solar greenhouses. *Biosystems Engineering*, Vol. 220, Issue 6, pp. 214-232. England. DOI: https://doi.org/10.1016/j.biosystemseng.2022.06.003

[16] Wang, C., Xu Z., Jiang, Y., Bai, Y., & Wang, T., (2023). Numerical analysis of static and dynamic characteristics of large-span pipe-framed plastic greenhouses. *Biosystems Engineering*, Vol. 232, No. 6, pp. 67-80, England. DOI: https://doi.org/10.1016/j.biosystemseng.2023.06.013

[17] Wang C., Shen J., Jiang Y., Zhu L., (2025). Failure mechanisms and reinforcement of pipe-framed solar greenhouses under snow loads. *Scientific reports*. Vol. 15, No.16403. England. DOI: https://doi.org/10.1038/s41598-025-01186-w

[18] Xie H., Wei C., Zheng X., Xu W., (2025). Stability analysis of flat-elliptical greenhouse skeleton considering initial geometrical imperfections. *INMATEH - Agricultural Engineering*, Vol. 75, No. 1, pp. 369-379, Bucharest/Romania. DOI: https://doi.org/10.35633/inmateh-76-31

[19] Xie Q., Ren J., (2025). Research on greenhouse planting density of landscape flowers in cold regions based on CFD simulation, *INMATEH - Agricultural Engineering*, Vol. 75, No. 1, pp. 469-479, Bucharest/Romania. DOI: https://doi.org/10.35633/inmateh-75-40

[20] Yan, D., Hu L., Zhou C., Yan J., (2022). Analysis of the performance of the oval tube arch of single-tube solar greenhouses. *Transactions of the Chinese Society of Agricultural Engineering.* Vol. 38, No. 5, pp. 217-224, Beijing/China. DOI: https://doi.org/10.11975/j.issn.1002-6819.2022.05.026